

# Dynamic Target Zone Modulation for Physical Activity Management in Artificial Pancreas Using Pulsatile Zone Model Predictive Control

Nicola Licini<sup>1</sup>, Roberto Trevisan, Giuseppe Lepore<sup>2</sup>, Fabio Previdi<sup>3</sup>, *Member, IEEE*,  
and Antonio Ferramosca<sup>4</sup>, *Senior Member, IEEE*

**Abstract**—Physical activity (PA) presents a significant challenge for artificial pancreas (AP) systems in managing Type 1 Diabetes, primarily by elevating the risk of hypoglycemia both during and after exercise. This work introduces and evaluates a novel exercise-aware pulsatile zone model predictive control (pZMPC) strategy designed to enhance glycemic safety and control around PA; in this proposal, the controller proactively mitigates this risk by dynamically modulating glucose target zones, elevating the target in anticipation of, during, and following announced PA. The performance of this strategy was systematically evaluated through in silico simulations across a cohort of ten virtual adult patients, under various scenarios designed to mimic real-life events, and using two control-relevant metabolic models, one of which explicitly accounted for exercise effects as an uncontrollable input. Compared to a standard pZMPC controller without exercise-specific adaptations, the proposed pZMPC with dynamic target zone modulation demonstrated an improvement in glycemic safety, reducing the incidence and duration of exercise-induced hypoglycemia. Furthermore, the strategy successfully decreased overall glycemic variability and maintained robust control even in the presence of uncertainties in PA information.

**Index Terms**—Artificial pancreas (AP), model predictive control (MPC), physical activity (PA), type 1 diabetes (T1D), varying target.

## I. INTRODUCTION

TYPE 1 diabetes mellitus (T1D) is characterized by autoimmune destruction of pancreatic  $\beta$ -cells, necessitating lifelong exogenous insulin therapy to maintain blood glucose (BG) within safe ranges [1]. Artificial pancreas (AP)

systems combine the sensing of a continuous glucose monitoring (CGM) sensor, the actuation of a subcutaneous insulin pump, and a control algorithm to compute the subject's needed amount, aiming to automate insulin delivery and reduce the burden of manually computing the insulin needs. Among control strategies, model predictive control (MPC) is particularly effective thanks to the explicit handling of multivariable dynamics, constraints, and predictions over a finite horizon, enabling principled tradeoffs between glycemic performance and safety [2]. Despite the robust predictive capability of MPC, BG control is extremely challenging due to factors such as intrasubject variability, delay between insulin administration and its metabolic action, measurement delays and noise introduced by CGM sensors, and physiological perturbations like meals and physical activity (PA). Particularly, this latter remains one of the most critical real-life burdens: aerobic exercise acutely increases glucose utilization [3] and augments insulin sensitivity (IS) [4], [5], elevating the risk of hypoglycemia during and in the prolonged recovery phase that follows. This challenge persists even with automated systems, primarily because current control actions focus mainly on lowering BG levels using insulin alone, which can exacerbate the effects of PA if this is not managed in advance. In practice, clinicians often recommend temporary strategies to mitigate this risk, including preemptive reductions of insulin delivery or proactively raising the patient's BG levels through fast-acting carbohydrates called hypoglycemic treatments (HT) [6]. In closed-loop control, these clinical heuristics should be embedded in a structured, predictive framework that can act on partial, uncertain, or delayed information about upcoming PA.

### A. Contributions

An exercise-aware AP strategy is developed within a pulsatile zone MPC (pZMPC) framework. The key idea is to dynamically modulate the controller's glucose target zone before, during, and after the announced PA event so that, when hypoglycemia risk is higher, the controller targets a higher BG range to proactively mitigate insulin delivery in a transparent and clinically interpretable manner. Safety is further reinforced through a nonstandard insulin-on-board (nsIOB) constraint [7] that limits insulin accumulation using a time-varying upper bound; the basal (fasting) allowance is adaptively relaxed when meal announcements occur and tightened afterward. PA information enters the controller through a

Received 3 December 2025; revised 10 March 2026; accepted 14 March 2026. This work was funded by the National Plan for NRRP Complementary Investments (PNC, established with the decree-law 6 May 2021, n. 59, converted by law n. 101 of 2021) in the call for the funding of research initiatives for technologies and innovative trajectories in the health and care sectors (Directorial Decree n. 931 of 06-06-2022) - project n. PNC0000003 - AdvanCed Technologies for Human-centred Medicine (project acronym: ANTHEM). This work reflects only the authors' views and opinions, neither the Ministry for University and Research nor the European Commission can be considered responsible for them - CUP B53C22006700001. Recommended by Associate Editor A. Mesbah. (*Corresponding author: Nicola Licini.*)

Nicola Licini, Fabio Previdi, and Antonio Ferramosca are with the Department of Management, Information and Production Engineering, University of Bergamo, Bergamo, 24044 Dalmine, Italy (e-mail: nicola.licini@unibg.it; previdi@unibg.it; antonio.ferramosca@unibg.it).

Roberto Trevisan and Giuseppe Lepore are with the Endocrine and Diabetology Unit, ASST Papa Giovanni XXIII, 24127 Bergamo, Italy (e-mail: rtrevisan@asst-pg23.it; glepore@asst-pg23.it).

Digital Object Identifier 10.1109/TCST.2026.3676649

unified representation that accommodates both preannounced (programmed) and at-onset (nonprogrammed) exercise without changing the optimization structure. The effect of this approach is then demonstrated in silico on a cohort of ten adult virtual subjects from the UVA/Padua simulator [8], using clinically grounded scenarios with variability in meal timing/size and exercise timing/intensity, and evaluating performance with two models: one that does not consider PA effect, based on the work by [9], to solely assess the effect of the variation in target, and one that considers PA as a new disturbance input, based on the work by [10].

### B. Paper Organization

This article is organized as follows. Section II reviews the current state of the art in PA management for T1D, motivating the need for the adaptive control proposal. Sections III and IV formally present our proposed exercise-aware pZMPC framework, detailing the dynamic target zone modulation strategy and the formulation of the optimization problem. Subsequently, Section V provides in silico evaluation of the proposed controller's performance and safety across a cohort of ten virtual patients under various exercise and meal scenarios. Finally, Section VI summarizes the key findings of this work and discusses potential avenues for future research and clinical translation. Throughout this article, boldface symbols denote vectors, while scalars are written in regular font.

## II. STATE OF THE ART IN PA MANAGEMENT

PA substantially alters glucose turnover and insulin requirements in T1D, creating distinctive risks during exercise and in recovery. Consensus guidance [6] emphasizes coordinated strategies spanning insulin adjustment, carbohydrate timing, and prudent use of diabetes technologies. This section synthesizes clinically grounded recommendations and technology directions, aligning them with the overall aim of exercise-aware closed-loop control.

### A. Clinical and Physiological Patterns Across Exercise Types

Understanding how different exercise modalities affect metabolic responses in T1D is fundamental to informing appropriate insulin and nutritional management. Aerobic PA (e.g., walking, cycling, jogging, and swimming) generally lowers glycemia during activity and increases hypoglycemia risk in recovery due to sustained IS changes [11]. Even with basal reductions, circulating insulin may not fall rapidly at exercise onset, contributing to early drops in glucose during light-to-moderate continuous exercise. Conversely, brief high-intensity or predominantly anaerobic efforts (sprints, heavy resistance sets, and intervals) often raise glycemia acutely via counterregulatory responses, with possible delayed hypoglycemia later [12]. Mixed or intermittent activities (e.g., team sports and intervals) frequently produce more stable intra-exercise glycemia than continuous aerobic work, yet recovery risk persists. These modality-dependent trends motivate proactive adjustments that account for intensity, duration, timing versus meals/insulin, and individual fitness [13].

### B. Practical Management Strategies From Consensus Guidance

Evidence-based guidance for safe PA in T1D emphasizes structured preparation, exercise-aware insulin adjustment, and carbohydrate strategies tailored to intensity, duration, and insulin-on-board (IOB). For aerobic sessions of approximately 1 h, beginning exercise near 126–180 [mg/dL] is commonly advised to mitigate intra-exercise hypoglycemia, whereas lower starting values may be acceptable for brief anaerobic or high-intensity interval exercise (HIIT), which often elicits transient hyperglycemic responses. When preexercise hyperglycemia is unexplained, capillary ketones should be assessed; the presence of elevated ketones warrants postponing activity and instituting corrective measures. Recent severe hypoglycemia constitutes a contraindication until fully resolved, reflecting the increased vulnerability to recurrent lows during subsequent activity [14]. Insulin adjustments are anchored to timing relative to meals and the expected exercise profile. For planned aerobic activity within roughly 60–90 min of a meal, preexercise prandial bolus reductions scaled to anticipated duration and intensity reduce hypoglycemia risk without necessitating large intraexercise carbohydrate loads [15]. Moreover, after afternoon exercise, particularly prolonged aerobic sessions, conservative overnight basal reductions or protective strategies are recommended to mitigate delayed hypoglycemia. In contrast, for brief anaerobic, resistance, or HIIT efforts, substantial preexercise insulin reductions are generally unnecessary; when postexercise hyperglycemia occurs, small conservative correction doses in early recovery are preferred over preemptive bolusing. Finally, during prolonged aerobic activity, in-session carbohydrate intake scaled by intensity and duration helps prevent hypoglycemia; normally, rapidly absorbable (high-glycemic index, i.e., glucose tabs or sugar/gel packets) sources are advantageous intraexercise when swift glycemic support is required [16]. Hence, glycemic adjustment prior to exercise remains difficult in practice, as insulin kinetics, exercise modality, timing relative to meals, and preceding glucose patterns interact in ways that complicate reliable decision-making.

### C. Algorithmic Approaches in AP Systems

Algorithmic handling of exercise in AP systems spans from reactive hypoglycemia protection to proactive, exercise-aware adaptation. At the reactive end, threshold suspend and predictive low-glucose suspend (PLGS) pause insulin when CGM glucose is low or predicted to fall, reducing intraexercise and nocturnal hypoglycemia; however, careful resume logic is essential to prevent postsuspend rebounds given subcutaneous insulin delays and counterregulatory variability [17]. Many systems also recommend fast-acting carbohydrate when glucose is dropping or predicted to drop, but this is framed as an emergency safety action rather than a coordinated control plan [18], [19]. Hybrid closed-loop (HCL) systems mitigate exercise-related hypoglycemia by incorporating user-initiated “exercise modes” that reduce basal delivery, cap insulin output, and raise glucose targets, sometimes coupled with carbohydrate prompts based on CGM trends and IOB [20].

Similarly, emerging fully closed-loop approaches integrate exercise awareness through manual announcements or wearable-derived signals (e.g., heart rate and accelerometry) [21]. In both cases, consensus guidelines recommend preexercise prandial bolus reductions and basal adjustments with sufficient lead time for aerobic sessions, while brief anaerobic or high-intensity efforts more often require conservative correction during recovery rather than preemptive insulin reduction. A complementary direction is the bihormonal AP, which adds a glucagon infusion channel to raise glucose when needed. This additional control input enables hypoglycemia prevention or correction without carbohydrate ingestion and has shown promise for improving overall glucose control compared with conventional insulin therapy and single-hormone AP in outpatient settings [22], [23], [24]. Despite these advances, its optimal use remains unsettled. While glucagon can support more aggressive insulin dosing, concerns arise from its reliance on hepatic glycogen, raising questions about whether it should be reserved for rescue or used routinely. Advances in stable, pump-compatible glucagon formulations reduce technical barriers, though long-term safety and efficacy data remain limited [25]. Recent modeling work [26] has improved the understanding of glucagon metabolic effects and could then be used in controller design.

Across single- and dual-hormone systems, layered safety remains a guiding principle: anticipate with temporary target elevation and insulin caps, protect with suspend/PLGS and conservative resumes, and, where available, apply cautious glucagon microdosing within defined safety limits.

### III. PROPOSED FRAMEWORK AND MODEL FOUNDATIONS

This work extends the layered safety paradigm depicted in Section II to the exercise domain by embedding it directly into an exercise-aware pulsatile Zone MPC. The controller dynamically modulates the glucose target before, during, and after PA to proactively mitigate hypoglycemia while maintaining robust overall control. The formulation integrates time-varying target zones with a segmented prediction horizon aligned to exercise phases and a unified event representation that consistently handles both preannounced and spontaneous activities without modifying the underlying optimization structure. In this section, we summarize the plant model used by the controller and provide a scheme of the phase segmentation that accounts for the PA effect.

#### A. Model Overview

To comprehensively evaluate our approach, we employ two distinct model variants: a five-state model that does not explicitly account for PA effects, and a seven-state extension that incorporates PA as an additional disturbance input. This dual-model assessment strategy allows us to first isolate the impact of target zone modulation alone (using the standard five-state model), and then to evaluate the combined effect of both target modulation and explicit PA-aware modeling (using the seven-state model).

The Ruan long-term minimal model [27], and its extension that captures insulin-independent effects of PA [10] are

therefore adopted. Both models' continuous-time state-space representations are described by

$$\begin{aligned}\dot{x}(t) &= Ax(t) + B_u u(t) + B_z z(t) + E \\ y(t) &= Cx(t)\end{aligned}\quad (1)$$

where  $x(t) \in \mathbb{R}^{n_x}$  are the system states ( $n_x = \{5, 7\}$  according to the model),  $u(t)$  is the insulin infusion rate [U/min] (controlled input), and  $z(t)$  stacks exogenous inputs, that is,  $z(t) = [r(t) \ p(t)]^\top$ , where  $r(t)$  is the meal rate [g/min] and  $p(t)$  is the PA profile [%VO<sub>2,max</sub>/min] (in the five-state model, where PA is not included,  $p(j)$  is omitted, so that  $z(j) = r(j)$ ). The measured output is  $y(t) = x_1(t)$ , corresponding to the BG concentration [mg/dL]. For paper readability, the full model matrices and parameter definitions are reported in Appendices A and B.

#### B. Event Announcement

Announced (or estimated) events are represented through the vector  $z(t) = [r(t) \ p(t)]^\top$ , where both  $r(j)$  and  $p(j)$  are sequences.

For meals of duration  $D_{rt}$ , we adopt a piecewise-constant approximation

$$r(j) = \begin{cases} \frac{\widehat{\text{CHO}}(j)}{D_{rt}}, & j \in \mathbb{I}_{0:n-1} \\ 0, & j \in \mathbb{I}_{n:N-1} \end{cases} \quad (2)$$

with integer duration  $n = \lfloor D_{rt}/T_s \rfloor$ .

For PA events, two scenarios are distinguished over the prediction horizon  $\mathbb{I}_{0:N-1}$  at time  $j$ : 1) *programmed* PA, where the trajectory is known to the controller in advance (e.g., scheduled exercise) and 2) *nonprogrammed* PA, where exercise is only announced/estimated at time  $j$  (i.e., not scheduled in advance). The corresponding profile for a PA event starting at time index  $t_{0,p}$  and lasting  $D_{pt}$  minutes, is defined as

$$p(j) = \begin{cases} 0, & j \in \mathbb{I}_{0:t_{0,p}-1} \\ \widehat{\text{PA}}(j), & j \in \mathbb{I}_{t_{0,p}:t_{0,p}+m-1} \\ 0, & j \in \mathbb{I}_{t_{0,p}+m:N-1} \end{cases} \quad (3)$$

with integer duration  $m = \lfloor D_{pt}/T_s \rfloor$ . To accommodate both scenarios, PA is parameterized by its start index  $t_{0,p}$ : in the programmed scenario,  $t_{0,p}$  is set to the scheduled start index within the horizon; in the nonprogrammed scenario, we set  $t_{0,p} = 0$  to indicate an immediate start at the current step.

*Remark 1:* We adopt the convention that  $\mathbb{I}_{a:b}$  is empty if  $a > b$  (e.g., when  $t_{0,p} = 0$ , the first condition in  $p(j)$  is inactive). If  $(t_{0,p} + m - 1) > N - 1$ , the active segment is implicitly truncated to the horizon.

#### C. PA Segment Selection

At each sampling instant  $j$ , the MPC solves an optimization over a prediction horizon of length  $N$  with indices  $\mathbb{I}_{0:N-1} \equiv \{0, 1, \dots, N-1\}$  measured relative to  $j$ , as it will be presented in Section IV. The phase selection below defines how the optimizer schedules the target zone *inside the prediction horizon* (cost and constraints).

Let the horizon be partitioned into three phases

$$N = N_{\text{pre}} + N_{\text{pa}} + N_{\text{post}}$$

with corresponding index sets

$$\mathbb{I}_{0:N-1} = \underbrace{\mathbb{I}_{0:N_{\text{pre}}-1}}_{\text{pre-PA}} \cup \underbrace{\mathbb{I}_{N_{\text{pre}}:N_{\text{pre}}+N_{\text{pa}}-1}}_{\text{during-PA}} \cup \underbrace{\mathbb{I}_{N_{\text{pre}}+N_{\text{pa}}:N-1}}_{\text{post-PA}}.$$

Given a PA event with start index  $t_{0,p}$  (within the prediction horizon) and duration  $m = \lfloor D_{pt}/T_s \rfloor$ , we introduce two additional parameters: 1) an anticipation window  $\kappa_{\text{pre}}$ , which allows the target to be elevated prior to the PA onset and 2) a recovery window  $\kappa_{\text{rec}}$ , which maintains the elevated target after the PA event. The start and end indices of the elevated-target segment are defined as

$$j_{\uparrow} = \begin{cases} \max\{0, t_{0,p} - \kappa_{\text{pre}}\}, & (\text{programmed PA}) \\ 0, & (\text{nonprogrammed PA}) \end{cases} \quad (4)$$

$$j_{\downarrow} = \min\{N, t_{0,p} + m + \kappa_{\text{rec}}\}. \quad (5)$$

Here,  $j_{\uparrow}$  marks the beginning of the target elevation, while  $j_{\downarrow}$  indicates when it returns to its nominal value. The elevated PA-target zone is hence applied in the optimization for all indices  $j \in \mathbb{I}_{j_{\uparrow}:j_{\downarrow}-1}$ ; outside this set, the nominal target zone is used. The segment lengths are then

$$N_{\text{pre}} = j_{\uparrow} \quad (6)$$

$$N_{\text{pa}} = \max\{0, j_{\downarrow} - j_{\uparrow}\} \quad (7)$$

$$N_{\text{post}} = N - N_{\text{pre}} - N_{\text{pa}}. \quad (8)$$

Hence, *within the prediction horizon*: 1) if the PA is programmed, the elevated segment begins  $\kappa_{\text{pre}}$  steps before  $t_{0,p}$  and 2) if the PA is nonprogrammed (at-onset), the elevation starts at the first predicted step ( $N_{\text{pre}} = 0$ ). In both cases, the elevated segment spans the exercise duration  $m$  and is prolonged by  $\kappa_{\text{rec}}$  steps to cover recovery.

*Remark 2*: If any segment length is zero (e.g.,  $N_{\text{pre}} = 0$ ), the corresponding index set is empty and the associated terminal constraint is inactive by convention. The clamping of  $j_{\uparrow}$  and  $j_{\downarrow}$  ensures proper truncation at the horizon boundaries: 1) if  $t_{0,p} - \kappa_{\text{pre}} \leq 0$ , then  $N_{\text{pre}} = 0$  (the anticipatory elevation starts immediately); 2) if  $t_{0,p} + m + \kappa_{\text{rec}} \geq N$ , then  $N_{\text{pa}} = N - N_{\text{pre}}$  and  $N_{\text{post}} = 0$ ; and 3) if the event lies entirely beyond the horizon, that is,  $t_{0,p} - \kappa_{\text{pre}} \geq N$ , then  $N_{\text{pre}} = N$  and  $N_{\text{pa}} = N_{\text{post}} = 0$ , meaning no target elevation occurs within the horizon.

#### IV. EXERCISE-AWARE pZMPC WITH SEGMENTED PREDICTION HORIZON

This section presents the pZMPC scheme for BG regulation under input and state constraints. The controller operates over a prediction horizon of length  $N$ , partitioned into the three contiguous segments described in Section III-C. Each segment incorporates phase-specific References, while terminal anchoring enforces continuity across phases. The control objective is to drive BG within the safety output zone  $\mathcal{Y}_{\text{Tar}}$ .

The scheme builds on a discrete-time pulsatile representation of the continuous model (1), following the discretization proposed in [9] and [10]. The formulation is characterized

by a sampling time  $T_s$  and a pulse duration  $\Delta T \leq T_s$ , and follows the MPC for tracking artificial variables framework to maintain properties of asymptotic stability and increased domain of attraction [28]. At each sampling instant  $k$ , the algorithm is initialized with the state estimate  $x(0) = \hat{x}(k)$ , provided by an output-disturbance observer (i.e., a Kalman filter based on an augmented model with a double-integrated disturbance, ensuring offset-free estimation in the presence of plant–model mismatch such as impulse, step, or ramp disturbances [9]).

##### A. Optimization Problem

Three key ingredients tailor the formulation to the application: 1) an asymmetric zone cost that penalizes hypoglycemic excursions more strongly than hyperglycemic ones; 2) an nsIOB constraint that adapts online to announced or estimated events, both taken from [7]; and 3) a time-varying target zone that adapts to PA.

The cost minimized at time  $k$  is the sum of a stage quadratic term ( $V_{\text{dyn}}$ ), which penalizes predicted glycemia with respect to the reference, and a stationary term ( $V_s$ ), which penalizes deviations of the terminal equilibrium from the target zones

$$V_N(\hat{x}, \hat{z}, \mathcal{Y}_{\text{Tar}}, \mathcal{Y}_{\text{Tar}}^{\text{PA}}; \Theta) = V_{\text{dyn}} + V_s \quad (9)$$

where  $\Theta = [\mathbf{u}, u_a, x_a, u_a^{\text{PA}}, x_a^{\text{PA}}, \delta_{\text{hyper}}, \delta_{\text{hypo}}, \delta_{\text{hyper},s}, \delta_{\text{hypo},s}, \delta_{\text{hyper},s}^{\text{PA}}, \delta_{\text{hypo},s}^{\text{PA}}]$  is the sequence of optimization variables. We enforce an asymmetric deviation with nonnegative slack variables  $\delta_{\text{hypo}}(j)$  and  $\delta_{\text{hyper}}(j)$  that bound the deviation of  $y(j)$  to  $y_{\text{ref}}(j)$  from below and above, respectively. The dynamic term reads

$$V_{\text{dyn}} = \sum_{j=0}^{N-1} \left( \|\delta_{\text{hypo}}(j)\|_{\tilde{Q}}^2 + \|\delta_{\text{hyper}}(j)\|_{\hat{Q}}^2 + \|u(j) - u_{\text{ref}}\|_R^2 \right) \quad (10)$$

with  $\tilde{Q} \gg \hat{Q} > 0$  to penalize hypoglycemia more heavily than hyperglycemia, and  $R > 0$  is the controllable input weight (i.e., insulin delivery). The stationary term steers the artificial equilibrium outputs into the admissible target zones: 1)  $\mathcal{Y}_{\text{Tar}} \doteq \{y \in \mathbb{R} : G_{\text{min}} - \delta_{\text{hypo},s} \leq y \leq G_{\text{max}} + \delta_{\text{hyper},s}\}$  and 2)  $\mathcal{Y}_{\text{Tar}}^{\text{PA}} \doteq \{y \in \mathbb{R} : G_{\text{min}}^{\text{PA}} - \delta_{\text{hypo},s}^{\text{PA}} \leq y \leq G_{\text{max}}^{\text{PA}} + \delta_{\text{hyper},s}^{\text{PA}}\}$ , via

$$V_s = \check{\rho} \left( (\delta_{\text{hypo},s})^2 + (\delta_{\text{hypo},s}^{\text{PA}})^2 \right) + \hat{\rho} \left( (\delta_{\text{hyper},s})^2 + (\delta_{\text{hyper},s}^{\text{PA}})^2 \right) \quad (11)$$

with nonnegative terminal slack variables. Choosing  $\check{\rho} \gg \hat{\rho}$  enforces preference for approaching the zone from above.

Hence, at each sampling instant  $k$ , the MPC solves

$$\begin{aligned} \min_{\Theta} V_N(\hat{x}, \hat{z}, \mathcal{Y}_{\text{Tar}}, \mathcal{Y}_{\text{Tar}}^{\text{PA}}; \Theta) \\ \text{s.t. } x(0) = \hat{x}(k) \end{aligned} \quad (12a)$$

$$\begin{aligned} x(j+1) = A^d x(j) + B_u^d u(j) + B_z^d z(j) \\ + E^d, j \in \mathbb{I}_{0:N-1} \end{aligned} \quad (12b)$$

$$y(j) = Cx(j), j \in \mathbb{I}_{1:N} \quad (12c)$$

$$x(j) \in \mathcal{X}(j; k), \quad u(j) \in \mathcal{U}, \quad j \in \mathbb{I}_{0:N-1} \quad (12d)$$

$$-\delta_{\text{hypo}}(j) \leq y(j) - y_{\text{ref}}(j) \leq \delta_{\text{hyper}}(j), \quad j \in \mathbb{I}_{1:N} \quad (12e)$$

$$y_{\text{ref}}(j) = \begin{cases} y_a, & j \in \mathbb{I}_{1:N_{\text{pre}}} \\ y_a^{\text{PA}}, & j \in \mathbb{I}_{N_{\text{pre}}+1:N_{\text{pre}}+N_{\text{pa}}} \\ y_a, & j \in \mathbb{I}_{N_{\text{pre}}+N_{\text{pa}}+1:N} \end{cases} \quad (12f)$$

$$u_{\text{ref}}(j) = \begin{cases} u_a, & j \in \mathbb{I}_{1:N_{\text{pre}}} \\ u_a^{\text{PA}}, & j \in \mathbb{I}_{N_{\text{pre}}+1:N_{\text{pre}}+N_{\text{pa}}} \\ u_a, & j \in \mathbb{I}_{N_{\text{pre}}+N_{\text{pa}}+1:N} \end{cases} \quad (12g)$$

$$x_a = \tilde{C}A^d x_a + \tilde{C}B_u^d u_a + \tilde{C}E^d, \quad y_a = x_{a,1} \quad (12h)$$

$$G_{\text{min}} - \delta_{\text{hypo}} \leq y_a \leq G_{\text{max}} + \delta_{\text{hyper}} \quad (12i)$$

$$x_a^{\text{PA}} = \tilde{C}A^d x_a^{\text{PA}} + \tilde{C}B_u^d u_a^{\text{PA}} + \tilde{C}E^d, \quad y_a^{\text{PA}} = x_{a,1}^{\text{PA}} \quad (12j)$$

$$G_{\text{min}}^{\text{PA}} - \delta_{\text{hypo}}^{\text{PA}} \leq y_a^{\text{PA}} \leq G_{\text{max}}^{\text{PA}} + \delta_{\text{hyper}}^{\text{PA}} \quad (12k)$$

$$x_a \in \tilde{\mathcal{C}}\mathcal{X}, \quad x_a^{\text{PA}} \in \tilde{\mathcal{C}}\mathcal{X}, \quad u_a \in \mathcal{U}, \quad u_a^{\text{PA}} \in \mathcal{U} \quad (12l)$$

$$x(N) = \begin{cases} x_a^{\text{PA}}, & \text{if } N_{\text{pa}} > 0 \text{ and } N_{\text{post}} = 0 \\ x_a, & \text{otherwise} \end{cases} \quad (12m)$$

$$\delta_{\text{hypo}}(j) \geq 0, \delta_{\text{hyper}}(j) \geq 0, \quad j \in \mathbb{I}_{1:N} \quad (12n)$$

$$\delta_{\text{hypo},s}, \delta_{\text{hyper},s}, \delta_{\text{hypo},s}^{\text{PA}}, \delta_{\text{hyper},s}^{\text{PA}} \geq 0. \quad (12o)$$

Constraint (12a) initializes the predicted state trajectory with the current estimate  $\hat{x}(k)$  provided by the state observer. The prediction dynamics (12b) and the output map (12c) are imposed over the horizon. The matrices  $A^d$ ,  $B_u^d$ ,  $B_z^d$ , and  $E^d$  denote the discrete-time versions of the continuous-time matrices  $A$ ,  $B_u$ ,  $B_z$ , and  $E$  in (1). The state constraint (12d) requires membership in a time-varying admissible set

$$\mathcal{X}(j;k) := \left\{ x \in \mathbb{R}_{\geq 0}^{n_x} \mid G_{\text{hypo}} \leq x_1(j) \leq G_{\text{hyper}}, \right. \\ \left. \theta_4(x_2(j) + x_3(j)) \leq \text{nsIOB}(j;k) \right\} \quad (13)$$

where  $\mathbb{R}_{\geq 0}^{n_x}$  denotes componentwise nonnegativity,  $G_{\text{hypo}}$  and  $G_{\text{hyper}}$  bound glucose  $x_1$ , and  $\theta_4(x_2 + x_3)$  is the model-based IOB estimate constrained by the nsIOB envelope  $\text{nsIOB}(j;k)$  (see Appendices A and B for details). The latter is computed online at time  $k$  and propagated over  $j \in \mathbb{I}_{0:N-1}$ . All remaining states  $x_4, \dots, x_{n_x}$  are unbounded beyond nonnegativity.

Insulin delivery is bounded in (12d) by the actuator limits, through the set

$$\mathcal{U} := \left\{ u \in \mathbb{R}_{\geq 0} \mid u \leq U_{\text{max}} \right\} \quad (14)$$

where  $U_{\text{max}}$  is the maximum deliverable insulin by the pump.

The zone constraint (12e) imposes an asymmetric soft band around the reference output  $y_{\text{ref}}(j)$ , with nonnegative slack variables  $\delta_{\text{hypo}}(j)$  and  $\delta_{\text{hyper}}(j)$  allowing temporary, penalized deviations. The references  $y_{\text{ref}}(j)$  and  $u_{\text{ref}}(j)$  are generated by (12f) and (12g) as a convex combination of “rest” and “PA” equilibrium points, piecewise references over the three horizon segments.

The equalities (12h)–(12j) define artificial steady states and inputs for the controlled subspace under rest and PA, respectively. We distinguish the controlled substate  $x_c := \tilde{C}x = [x_1, x_2, x_3]^T$  via  $\tilde{C} = [I_3 \ 0_{3 \times (n_x-3)}]$ , since insulin delivery directly influences only these three states. In this sense, only the controllable states are steered to the controllable target through the artificial references of the controller.

The bounds (12i)–(12k) keep steady-state outputs within clinically acceptable glucose ranges [with terminal slacks  $\delta_{\text{hypo},s}$ ,  $\delta_{\text{hyper},s}$ , and their PA counterparts as per (12o)].

Feasibility of these steady points is ensured by (12l), requiring  $x_a, x_a^{\text{PA}} \in \mathcal{X}$  and  $u_a, u_a^{\text{PA}} \in \mathcal{U}$ .

Constraint (12m) imposes a single phase-dependent terminal equality at the end of the prediction horizon: the optimizer anchors to the PA equilibrium if and only if the elevated PA segment reaches the horizon tail (i.e.,  $j_{\uparrow} < j_{\downarrow} = N$ , equivalently  $N_{\text{pa}} > 0$  and  $N_{\text{post}} = 0$ ); otherwise it anchors to the rest equilibrium  $x_a$ . At the same time, it leaves the states at  $N_{\text{pre}}$  and  $N_{\text{pre}} + N_{\text{pa}}$  unconstrained so the optimizer can transition smoothly across phases.

Once the optimization is solved, the receding-horizon control law applies the first input of the optimal sequence,  $\kappa_{\text{MPC}}(\hat{x}, \hat{z}, \mathcal{Y}^{\text{Tar}}) = u^*(0; x)$ , and the problem is shifted and resolved at the next sampling instant with new glucose measurements.

1) *nsIOB Constraint*: Within the state constraint set  $\mathcal{X}$ , insulin-related states  $x_2$  and  $x_3$  are limited by a time-varying nsIOB envelope  $\text{nsIOB}(j;k)$ , computed online at each sampling instant  $k$ , and propagated across the prediction horizon  $j \in \mathbb{I}_{0:N-1}$ , following [7]. The construction assumes superposition of basal (fasting) and bolus (postprandial) insulin effects: the input  $u(t)$  is decomposed into basal,  $U_b$ , that is, at fasting, and meal-bolus  $u_{pp}(t)$  components whose actions add linearly in the states; it follows that the  $\text{IOB}(t) = \theta_4(x_2(t) + x_3(t))$  could be rewritten as  $\text{IOB}(t) = \theta_4(x_{2,b} + x_{2,pp}(t) + x_{3,b} + x_{3,pp}(t)) = \theta_4 \cdot 2U_b + \text{IOB}_{pp}(t)$ .

In the formulation of the constraints, the envelope mirrors this decomposition. In the absence of announced events, the IOB upper bound is the constant basal value  $\text{IOB}_b = \theta_4 \cdot 2U_b$ . When a meal is announced/detected at discrete time  $k_0$  with estimated carbohydrate content  $\widehat{\text{CHO}}_0$ , the bound is relaxed over the postprandial period according to

$$\text{nsIOB}(j;k_0) = \text{IOB}_b + \text{IOB}_{pp}\left(k_0 + j; k_0, \widehat{\text{CHO}}_0\right) \\ j \in \mathbb{I}_{0:N-1} \quad (15)$$

where  $\text{IOB}_{pp}(k_0 + j; k_0, \widehat{\text{CHO}}_0)$  is a meal-size-dependent, time-decaying contribution scaled by the associated bolus  $U_0 = \widehat{\text{CHO}}_0/\text{CR}$ . Consistent with [7], the postprandial component is active over a fixed window  $\Delta T_{\text{IOB}}$  (e.g.,  $\Delta T_{\text{IOB}} = 60$  min) common to all patients, after which the envelope reverts to its basal value. This design limits insulin accumulation via  $\theta_4(x_2 + x_3)$  while adaptively permitting higher IOB for a prolonged interval following announced meals, due to the possibility of error in their announcement.

2) *MPC Formulation—Recursive Feasibility*: To guarantee recursive feasibility in the presence of meals, PA, and model mismatch, we relax selected hard constraints using nonnegative slack variables that are explicitly penalized in the cost [29]. This applies both along the prediction horizon (dynamic zone-tracking) and at the terminal (stationary zone) level, while preserving hard bounds where structurally required (e.g., input limits and nonnegativity of states).

The admissible state set  $\mathcal{X}(j;k)$  is in this way relaxed as

$$G_{\text{hypo}} - \delta_{\text{hypo}}(j) \leq x_1(j) \leq G_{\text{hyper}} + \delta_{\text{hyper}}(j) \\ 0 \leq \theta_4(x_2(j) + x_3(j)) \leq \text{nsIOB}(j;k) + \delta_{\text{IOB}}(j)$$

TABLE I

MEAL SCHEDULE; EACH MEAL IS CHARACTERIZED BY A VARIABILITY OF  $\pm 10$  MIN IN TIMING AND DURATION, AND  $\pm 20\%$  SIZE

Meal	Nominal time	Carbs [g]	Duration [min]
Breakfast	07:00	60	30
Lunch	12:00	60	30
Dinner	18:00	80	40

TABLE II

PA TEMPLATES USED IN SIMULATIONS. INTENSITIES ARE EXPRESSED AS FRACTIONS OF  $VO_{2\max}$ . EACH EVENT INCLUDES A VARIABILITY OF  $\pm 10$  MIN IN TIMING AND  $\pm 20\%$  IN INTENSITY

Total duration	Phase sequence
45 min	10 min light (25%), 10 min high (65%), 20 min moderate (50%), 5 min light (25%).
90 min	5 min light (25%), 10 min moderate (50%), 10 min high (65%), 25 min moderate (50%), 10 min high (65%), 15 min moderate (50%), 15 min light (25%).

to prevent infeasibility in scenarios where transient glycemia or IOB accumulation would otherwise violate the envelope. In all cases,  $\delta_{\text{hypo}}(j) \geq 0$ ,  $\delta_{\text{hyper}}(j) \geq 0$ , and  $\delta_{\text{IOB}}(j) \geq 0$  are nonnegative slack variables, weighted through a quadratic penalty term in the cost function to discourage their activation.

At the terminal level, feasibility of the artificial steady outputs that underpin the phase selectors (rest and PA) is guaranteed via zone slacks  $\delta_{\text{hypo},s}$ ,  $\delta_{\text{hyper},s}$  and their PA counterparts  $\delta_{\text{hypo},s}^{\text{PA}}$ , and  $\delta_{\text{hyper},s}^{\text{PA}}$ , which softly confine  $y_a$  and  $y_a^{\text{PA}}$  within their respective bands (elevated during PA). Because  $x_a$  and  $x_a^{\text{PA}}$  (and their inputs) are decision variables constrained only by these softened terminal zones, the terminal equalities at segment boundaries are always satisfiable; if a segment is empty, its terminal condition is inactive by convention. With all slacks explicitly penalized, the standard shift–append receding-horizon argument provides a feasible successor at the next step, thereby maintaining feasibility across pre-PA, during-PA, and post-PA transitions without redefining the optimization.

## V. RESULTS AND DISCUSSION

The proposed pZMPC was evaluated in silico on a cohort of ten adult virtual subjects drawn from the FDA-approved UVA/Padua simulator for research [30], embedding PA following the framework proposed in [31]. The controller was implemented in MATLAB and solved using YALMIP [32].

### A. Description of Scenarios

Each simulation spanned 14 days. The daily events are resumed in Tables I and II. The meal plan comprised three nominal meals (60 g at 07:00, 60 g at 12:00, and 80 g at 18:00), with durations set to 30 min for breakfast and lunch and 40 min for dinner as in [9]. To better mimic real-life scenarios, randomized variability was added to the events in timing ( $\pm 10$  min), size ( $\pm 20\%$ ), and duration ( $\pm 10$  min).

PA was simulated with two different workout sessions expressed as fractions of  $VO_{2\max}$ . The first one is a 45-min routine consisting of: 10 min light (25%), 10 min high (65%),

20 min moderate (50%), and 5 min light (25%). The second one is a 90-min routine followed: 5 min light (25%), 10 min moderate (50%), 10 min high (65%), 25 min moderate (50%), 10 min high (65%), 15 min moderate (50%), and 15 min light (25%). Sessions were scheduled between 06:00 and 22:00, always at least 45 min after any meal, and alternated with rest days, consistent with ADA advice [33]. To reflect day-to-day variability, PA phase durations and intensities (light, moderate, and high) were perturbed by  $\pm 20\%$ , and the overall session start time was shifted by  $\pm 10$  min. Both programmed and nonprogrammed PA cases were exercised as defined previously in Section IV.

Sensing and actuation are consistent with common clinical devices; glucose was measured using the model corresponding to the Dexcom G5 Mobile CGM, proposed in [34]. The simulator’s default insulin pump was used [35], with a maximum deliverable insulin of  $U_{\max} = 15$  [U/min]. Insulin was delivered via pulses (both basal and bolus) of fixed width  $\Delta T_s = 1$  min. The MPC sampling time was  $T_s = 5$  min.

Stage costs were set to  $\hat{Q} = 1$ ,  $\check{Q} = 10^2$ , and  $R = 1$ ; asymmetric deviation penalties were  $\hat{\rho} = 10^6$  (hyperglycemia) and  $\check{\rho} = 10^9$  (hypoglycemia). The prediction horizon covered 6 h ( $N = 72$  steps), in line with ADA recommendations [36]. Within this horizon, the glucose target was increased during a possible preexercise anticipation window of  $\kappa_{\text{pre}} = [90 \text{ min}/T_s]$ , and then maintained for a recovery period of  $\kappa_{\text{rec}} = [120 \text{ min}/T_s]$  after the event. The same tuning was used for all ten adults except “Adult 7,” for whom  $\check{Q}$  was increased to  $10^3$  to account for a higher mean IS.

Finally, zone constraints were applied to the predictions as follows: the predicted glucose state  $x_1$  was bounded by  $G_{\text{hypo}} = 60$  mg/dL and  $G_{\text{hyper}} = 300$  mg/dL to prevent severe hypo and hyperglycemia. At the end of the horizon, predictions were driven to the target zone  $\mathcal{Y}_{\text{Tar}}$  with bounds  $G_{\text{min}} = 90$  mg/dL and  $G_{\text{max}} = 120$  mg/dL; when PA is active, the PA-specific target zone, higher than the basal one,  $\mathcal{Y}_{\text{Tar}}^{\text{PA}}$  with bounds  $G_{\text{min}}^{\text{PA}} = 126$  mg/dL and  $G_{\text{max}}^{\text{PA}} = 180$  mg/dL was used instead, since this range balances performance considerations against the risk of hypoglycemia [6].

To probe robustness, we tested increasing levels of complexity, including inaccuracies in event announcements (meals and PA) and circadian modulation of IS [37].

### B. Outcome Metrics and Result Visualization

We assess controller performance using CGM-derived glycemic indices and insulin usage measures [38]. Unless otherwise specified, all metrics are computed over the full simulation horizon for each virtual subject and then summarized across the cohort as median and interquartile range [25th, 75th percentile]. The indices considered include: mean glucose ( $\bar{G}_m$ ); glucose standard deviation (SD); coefficient of variation  $\text{CV}(\%) = 100 \cdot \text{SD}/\bar{G}_m$ ; percentages of time in the euglycemic range 70–180 mg/dL ( $T_{70-180}$ ) and in the tighter euglycemic range 70–140 mg/dL ( $T_{70-140}$ ); percentages of time above 180 and 250 mg/dL ( $T_{>180}$  and  $T_{>250}$ , respectively); percentages of time below 70 and 54 mg/dL ( $T_{<70}$  and  $T_{<54}$ , respectively); and total daily insulin (TDI) [U/day].

TABLE III  
 OUTCOME METRICS UNDER PERFECTLY ANNOUNCED DISTURBANCES WITHOUT IS VARIATION.  
 LEFT: FIVE-STATE MODEL; RIGHT: SEVEN-STATE MODEL

Metric	Five-state model			Seven-state model			
	Fixed	Var-Prog	Var-NonProg	Fixed-Prog	Fixed-NonProg	Var-Prog	Var-NonProg
$G_m$ [mg/dL]	119.0 [116.1, 122.9]	120.4 [119.2, 123.6]	119.5 [117.1, 123.4]	118.0 [116.3, 120.0]	116.1 [114.7, 119.1]	120.2 [118.4, 121.4]	116.3 [114.7, 119.1]
SD [mg/dL]	31.4 [23.4, 32.7]	30.6 [23.1, 31.7]	30.6 [23.0, 32.1]	28.0 [22.1, 30.7]	29.7 [22.7, 32.2]	28.9 [22.2, 30.9]	29.6 [22.7, 32.2]
CV [%]	26.2 [20.3, 27.9]	25.1 [19.0, 26.4]	25.6 [19.8, 27.1]	24.4 [19.4, 26.1]	26.1 [20.2, 27.6]	24.5 [19.1, 25.7]	26.0 [20.2, 27.6]
$T_{70-140}$ [%]	75.1 [71.2, 79.0]	76.0 [71.5, 79.5]	75.5 [71.8, 79.4]	78.8 [76.1, 82.4]	77.1 [75.4, 82.7]	78.6 [75.4, 81.8]	77.1 [75.4, 82.7]
$T_{70-180}$ [%]	92.2 [90.3, 96.1]	93.0 [91.0, 96.0]	93.1 [90.7, 96.5]	96.5 [92.8, 98.1]	94.6 [90.8, 97.0]	96.0 [92.8, 97.4]	94.8 [90.8, 96.8]
$T_{>180}$ [%]	3.5 [1.4, 7.0]	4.0 [2.3, 7.6]	3.6 [1.7, 6.9]	2.6 [1.2, 5.9]	2.0 [1.0, 5.8]	3.9 [2.3, 6.9]	2.1 [0.9, 5.8]
$T_{>250}$ [%]	0.0 [0.0, 0.0]	0.0 [0.0, 0.0]	0.0 [0.0, 0.0]	0.0 [0.0, 0.0]	0.0 [0.0, 0.0]	0.0 [0.0, 0.0]	0.0 [0.0, 0.0]
$T_{<70}$ [%]	2.7 [1.9, 3.7]	1.4 [0.9, 2.6]	2.3 [1.4, 3.2]	1.0 [0.4, 1.4]	2.3 [1.4, 3.3]	0.2 [0.0, 0.4]	2.2 [1.4, 3.3]
$T_{<54}$ [%]	1.5 [0.6, 2.4]	0.5 [0.1, 0.9]	1.1 [0.3, 1.8]	0.1 [0.0, 0.3]	1.2 [0.5, 1.6]	0.0 [0.0, 0.0]	1.1 [0.5, 1.6]
TDI [U]	42.1 [37.7, 50.7]	41.5 [37.3, 50.2]	41.9 [37.6, 50.6]	42.3 [38.0, 52.7]	42.4 [38.1, 52.8]	41.8 [37.4, 51.9]	42.4 [38.1, 52.8]

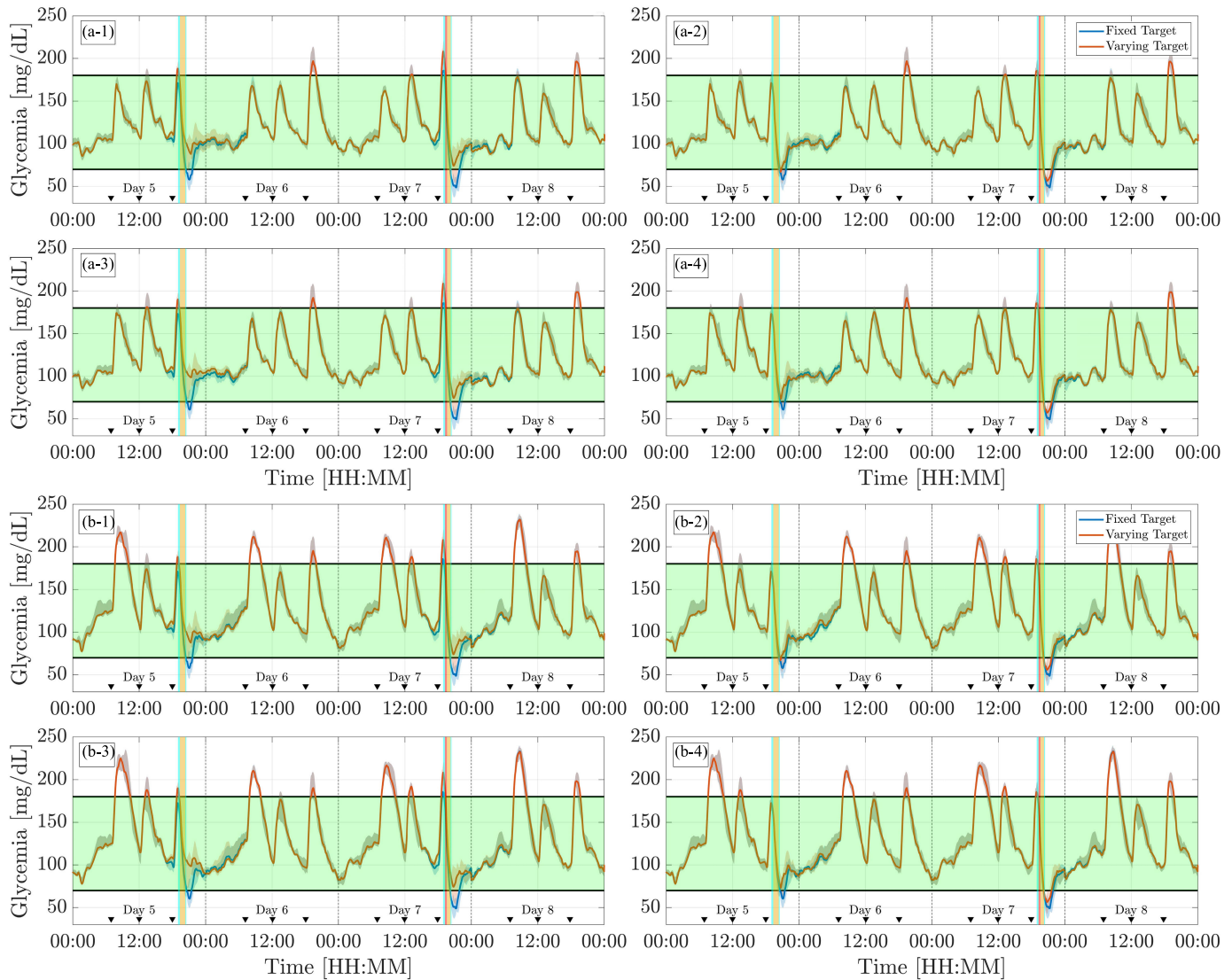


Fig. 1. Closed-loop simulation of the five-state model zoomed over 4 days. Each compares the proposed varying target (red) with the fixed-target controller (blue). Solid lines indicate the cohort median glucose, and shaded areas represent the interquartile range. Vertical colored lines denote PA, with each color corresponding to a different intensity. (a-1)–(a-4) Shows results without circadian IS variation and (b-1)–(b-4) includes this variation. Within each row, (a-1), (a-3), (b-1), and (b-3) correspond to programmed PA, and (a-2), (a-4), (b-2), and (b-4) to nonprogrammed PA. Perfectly announced disturbances are shown in (a-1), (a-2), (b-1), and (b-2), whereas erroneously announced disturbances are shown in (a-3), (a-4), (b-3), and (b-4).

### C. Results by Scenario

We summarize outcomes across four scenarios that combine the accuracy of event announcements (perfect versus erroneous) with the presence or absence of circadian IS variation.

For each scenario, the comparison tables present the five-state model (left block) and the seven-state model (right block), contrasting fixed and varying target strategies under *programmed* and *nonprogrammed* PA.

TABLE IV  
OUTCOME METRICS UNDER ERRONEOUSLY ANNOUNCED DISTURBANCES WITHOUT IS VARIATION.  
LEFT: FIVE-STATE MODEL; RIGHT: SEVEN-STATE MODEL

Metric	Five-state model			Seven-state model			
	Fixed	Var-Prog	Var-NonProg	Fixed-Prog	Fixed-NonProg	Var-Prog	Var-NonProg
$\bar{G}_m$ [mg/dL]	119.2 [116.3, 123.5]	121.0 [119.3, 124.2]	119.7 [117.3, 123.9]	117.8 [115.6, 119.2]	115.9 [114.8, 118.4]	120.2 [118.8, 120.7]	116.3 [115.4, 118.9]
SD [mg/dL]	31.7 [23.7, 32.8]	30.9 [23.3, 31.7]	30.9 [23.3, 32.2]	29.2 [22.2, 31.9]	30.0 [23.0, 32.2]	29.9 [22.9, 32.4]	30.1 [23.1, 32.4]
CV [%]	26.4 [20.5, 27.9]	25.4 [19.5, 26.6]	25.6 [20.1, 27.4]	25.5 [19.7, 26.8]	26.4 [20.6, 27.8]	25.3 [19.8, 27.0]	26.3 [20.6, 27.9]
$T_{70-140}$ [%]	75.0 [71.1, 78.6]	75.9 [71.3, 79.2]	75.5 [71.6, 79.2]	78.4 [74.9, 82.8]	77.0 [75.1, 82.9]	77.8 [74.6, 81.7]	76.9 [75.3, 82.4]
$T_{70-180}$ [%]	91.9 [89.9, 96.0]	92.6 [91.1, 95.9]	92.8 [90.1, 96.5]	95.3 [92.2, 98.1]	94.6 [91.0, 97.0]	95.0 [92.1, 97.3]	94.6 [91.0, 96.6]
$T_{>180}$ [%]	4.0 [2.0, 7.3]	4.5 [2.6, 7.8]	4.0 [2.0, 7.4]	3.1 [1.4, 6.1]	2.3 [1.1, 5.9]	4.4 [2.4, 7.1]	2.5 [1.1, 6.1]
$T_{>250}$ [%]	0.0 [0.0, 0.0]	0.0 [0.0, 0.0]	0.0 [0.0, 0.0]	0.0 [0.0, 0.0]	0.0 [0.0, 0.0]	0.0 [0.0, 0.0]	0.0 [0.0, 0.0]
$T_{<70}$ [%]	2.6 [1.9, 3.7]	1.5 [0.8, 3.0]	2.3 [1.3, 3.1]	1.6 [0.7, 1.9]	2.6 [1.6, 3.1]	0.6 [0.3, 0.8]	2.3 [1.4, 2.9]
$T_{<54}$ [%]	1.6 [0.7, 2.4]	0.7 [0.1, 1.2]	1.1 [0.5, 1.6]	0.5 [0.3, 0.8]	1.4 [0.5, 1.6]	0.1 [0.0, 0.4]	1.2 [0.4, 1.5]
TDI [U]	42.1 [37.7, 50.7]	41.5 [37.3, 50.2]	41.9 [37.6, 50.6]	42.4 [37.9, 52.9]	42.5 [38.2, 53.1]	41.8 [37.4, 52.0]	42.4 [38.2, 52.9]

TABLE V  
OUTCOME METRICS UNDER PERFECTLY ANNOUNCED DISTURBANCES WITH IS VARIATION.  
LEFT: FIVE-STATE MODEL; RIGHT: SEVEN-STATE MODEL

Metric	Five-state model			Seven-state model			
	Fixed	Var-Prog	Var-NonProg	Fixed-Prog	Fixed-NonProg	Var-Prog	Var-NonProg
$\bar{G}_m$ [mg/dL]	127.7 [124.5, 134.1]	129.2 [126.4, 135.1]	128.2 [125.2, 134.5]	128.7 [124.3, 130.2]	127.0 [123.1, 129.1]	130.8 [126.2, 131.9]	127.3 [123.5, 129.4]
SD [mg/dL]	39.9 [35.4, 43.0]	38.9 [34.7, 41.9]	39.3 [35.0, 42.4]	38.5 [34.3, 40.4]	39.3 [35.1, 41.7]	38.0 [33.8, 40.4]	39.4 [35.3, 41.9]
CV [%]	31.3 [28.4, 33.1]	30.1 [27.1, 31.6]	30.6 [27.9, 32.4]	29.9 [27.6, 31.6]	30.9 [28.3, 33.2]	29.1 [26.8, 31.1]	30.9 [28.5, 33.2]
$T_{70-140}$ [%]	66.5 [64.3, 71.1]	67.6 [65.0, 71.5]	67.1 [65.2, 71.4]	69.8 [69.2, 72.6]	69.6 [67.5, 71.9]	69.2 [67.5, 72.7]	69.3 [67.4, 71.7]
$T_{70-180}$ [%]	83.0 [81.2, 86.0]	84.4 [82.0, 86.0]	83.8 [82.2, 86.3]	86.2 [84.2, 88.8]	84.2 [83.2, 87.7]	86.0 [84.1, 89.1]	84.1 [83.1, 87.6]
$T_{>180}$ [%]	12.7 [11.2, 14.6]	13.0 [11.7, 15.1]	12.8 [11.2, 14.6]	11.7 [9.1, 14.2]	11.6 [9.2, 14.2]	12.8 [9.8, 15.3]	11.8 [9.5, 14.3]
$T_{>250}$ [%]	0.0 [0.0, 0.1]	0.0 [0.0, 0.1]	0.0 [0.0, 0.1]	0.0 [0.0, 0.1]	0.0 [0.0, 0.1]	0.0 [0.0, 0.1]	0.0 [0.0, 0.1]
$T_{<70}$ [%]	3.2 [2.7, 3.7]	1.9 [1.3, 2.5]	2.6 [1.8, 2.8]	1.6 [1.3, 2.1]	2.7 [2.1, 3.8]	1.0 [0.4, 1.8]	2.5 [1.9, 3.7]
$T_{<54}$ [%]	1.4 [0.8, 2.4]	0.5 [0.2, 1.0]	1.0 [0.3, 1.6]	0.2 [0.0, 0.4]	1.0 [0.5, 1.4]	0.0 [0.0, 0.2]	0.9 [0.5, 1.3]
TDI [U]	44.5 [40.0, 53.8]	44.0 [39.7, 53.4]	44.3 [39.9, 53.8]	44.6 [40.5, 55.3]	44.7 [40.8, 55.8]	44.1 [40.0, 54.5]	44.6 [40.7, 55.5]

1) *Scenario A: Perfectly Announced Disturbances:* Under conditions of perfect PA announcements, implementing a dynamic PA-dependent glucose target consistently mitigates hypoglycemia while maintaining a high proportion of time within the target range. The results are summarized in Table III.

Particularly, in the 1) five-state model, the varying target reduces both overall and severe hypoglycemia, with the most pronounced improvements observed during Programmed PA (e.g., reductions in  $T_{<70}$  from 2.7% to 1.4% and  $T_{<54}$  from 1.5% to 0.5%), while preserving the time in range ( $T_{70-180}$ ) and maintaining  $T_{>250}$  at zero. Mean glucose levels and insulin delivery remain comparable across targeting strategies.

In the 2) seven-state model, where PA dynamics are explicitly modeled, the safety margin further increases in the programmed setting:  $T_{<70}$  equals to 0.2% and  $T_{<54}$  to 0.0%, both declining substantially under the varying target. A small increase in  $T_{>180}$  reflects the expected safety-performance tradeoff, whereas time-in-range remains high and severe hyperglycemia is absent. For the nonprogrammed PA setting, the varying target strategy similarly demonstrates consistent improvements over the fixed target. Although the anticipatory elevation of the target zone is absent, reacting to the PA onset with a higher target still yields a clinically relevant reduction in hypoglycemic exposure (e.g.,  $T_{<70}$  drops from 2.3% to 2.2% in the seven-state model) while preserving high time-in-range, underscoring the strategy's utility even without anticipatory information.

Cohort trajectories for this scenario are shown in Figs. 1 (a-1), (a-2), (b-1), and (b-2) and 2(c-1), (c-2), (d-1), and (d-2). In both models, the varying target induces

anticipatory attenuation around PA events and produces tighter glucose envelopes during activity, particularly under programmed PA.

2) *Scenario B: Erroneously Announced Disturbances:* Under errors in both meal-size and PA-intensity announcements, summarized by Table IV, the varying PA-dependent target remains robust and continues to function primarily as a hypoglycemia-mitigating mechanism. The varying target decreases  $T_{<70}$  and  $T_{<54}$  in the 1) five-state model in the programmed PA condition, with only minimal effect on overall time-in-range. A modest increase in  $T_{>180}$  is observed, consistent with a safety-first design objective. In the 2) seven-state model, with the programmed setting, the varying target preserves a substantial reduction in hypoglycemia while keeping  $T_{70-180}$  nearly unchanged and producing only a mild rise in  $T_{>180}$ . The nonprogrammed case exhibits smaller but directionally consistent benefits. Glycemic variability and TDI remain broadly similar across targets. Trajectories of both models are shown in Figs. 1(a3), (a-4), (b-3), and (b-4) and 2(c3), (c-4), (d-3), and (d-4). Again, particularly under programmed PA, the varying target induces anticipatory attenuation around PA events and produces tighter glucose envelopes during activity, hence showing a maintained controller robustness under misannounced disturbances.

3) *Scenario C-D: Circadian Is Variation, With Perfect and Erroneous Disturbance Announcements:* Circadian fluctuations in IS increase the overall control challenge. Nevertheless, the varying PA-dependent target consistently enhances hypoglycemia protection under both perfect and erroneous disturbance announcements while maintaining clinically acceptable glycemic ranges.

TABLE VI  
OUTCOME METRICS UNDER ERRONEOUSLY ANNOUNCED DISTURBANCES WITH IS VARIATION.  
LEFT: FIVE-STATE MODEL; RIGHT: SEVEN-STATE MODEL

Metric	Five-state model			Seven-state model			
	Fixed	Var-Prog	Var-NonProg	Fixed-Prog	Fixed-NonProg	Var-Prog	Var-NonProg
$\bar{G}_m$ [mg/dL]	128.1 [124.9, 134.7]	129.6 [126.5, 135.6]	128.5 [125.4, 134.8]	128.9 [124.1, 130.0]	127.1 [123.0, 129.1]	130.9 [126.5, 132.0]	127.7 [123.7, 129.7]
SD [mg/dL]	40.1 [36.1, 43.6]	39.1 [35.5, 42.7]	39.6 [35.7, 43.1]	39.1 [34.8, 41.5]	39.6 [35.5, 42.6]	38.8 [34.4, 41.9]	39.7 [35.7, 42.7]
CV [%]	31.4 [29.0, 33.3]	30.2 [27.6, 31.8]	30.8 [28.5, 32.5]	30.4 [28.1, 32.8]	31.0 [28.6, 33.7]	29.6 [27.3, 32.3]	31.0 [28.9, 33.6]
$T_{70-140}$ [%]	66.1 [63.8, 70.7]	67.0 [64.0, 71.4]	66.7 [64.6, 70.6]	69.2 [67.0, 72.2]	69.7 [67.0, 71.9]	68.4 [67.2, 71.7]	69.2 [66.7, 71.7]
$T_{70-180}$ [%]	82.8 [80.6, 85.5]	84.0 [81.4, 85.8]	83.7 [81.3, 86.1]	85.0 [83.6, 88.2]	84.1 [83.0, 87.5]	85.0 [83.9, 88.7]	84.1 [82.8, 87.1]
$T_{>180}$ [%]	13.1 [11.4, 14.7]	13.4 [12.0, 15.3]	13.1 [11.4, 14.9]	12.2 [9.4, 14.7]	11.7 [9.4, 14.3]	13.1 [9.8, 15.4]	12.1 [9.8, 14.5]
$T_{>250}$ [%]	0.1 [0.0, 0.4]	0.1 [0.0, 0.4]	0.1 [0.0, 0.4]	0.0 [0.0, 0.2]	0.0 [0.0, 0.2]	0.1 [0.0, 0.2]	0.0 [0.0, 0.2]
$T_{<70}$ [%]	3.3 [2.7, 3.7]	1.9 [1.1, 2.9]	2.6 [2.0, 3.3]	2.2 [1.6, 2.9]	2.6 [2.3, 3.6]	1.3 [0.7, 1.8]	2.4 [1.9, 3.6]
$T_{<54}$ [%]	1.5 [0.7, 2.4]	0.7 [0.3, 1.0]	1.1 [0.5, 1.4]	0.5 [0.3, 0.8]	1.1 [0.5, 1.5]	0.1 [0.0, 0.4]	1.0 [0.5, 1.3]
TDI [U]	44.3 [39.9, 53.6]	43.8 [39.5, 53.3]	44.2 [39.8, 53.5]	44.6 [40.3, 55.4]	44.7 [40.6, 55.8]	44.0 [39.9, 54.5]	44.6 [40.5, 55.5]

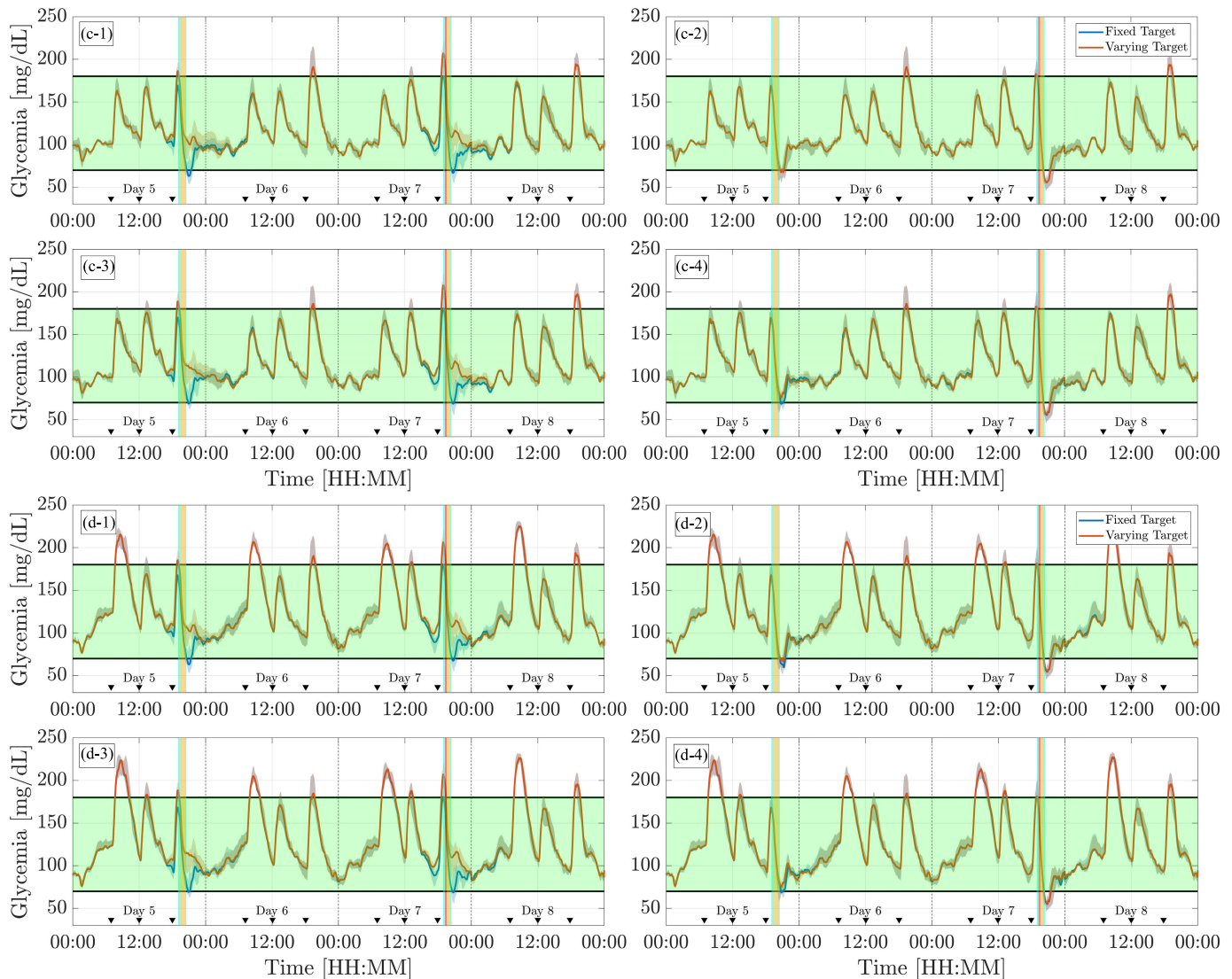


Fig. 2. Closed-loop simulation of the seven-state model zoomed over four days. Each compares the proposed varying target (red) with the fixed-target controller (blue). Solid lines indicate the cohort median glucose, and shaded areas represent the interquartile range. Vertical colored lines denote PA, with each color corresponding to a different intensity. (c-1)–(c-4) Shows results without circadian IS variation and (d-1)–(d-4) includes this variation. Within each row, (c-1), (c-3), (d-1), and (d-3) correspond to programmed PA, and (c-2), (c-4), (d-2), and (d-4) to nonprogrammed PA. Perfectly announced disturbances are shown in (c-1), (c-2), (d-1), and (d-2), whereas erroneously announced disturbances are shown in (c-3), (c-4), (d-3), and (d-4).

In the five-state model 1), with perfect announcements (Table V), the varying target reduces both  $T_{<70}$  and  $T_{<54}$ , causing only minor shifts in mean glucose and  $T_{>180}$ , and leaving  $T_{>250}$  essentially at zero. When announcement errors

are present (Table VI), these hypoglycemia benefits are largely preserved; the main tradeoff is a modest increase in time above range, while time-in-range, glycemic variability, and daily insulin usage remain within clinically acceptable limits.

When PA is explicitly modeled in the seven-state model 2), the varying target provides strong hypoglycemia mitigation, particularly during programmed PA (Table V). With perfect announcements, severe hypoglycemia is virtually eliminated, accompanied by only slight increases in mean glucose and  $T_{>180}$ , consistent with a safety-first approach. Under announcement errors (Table VI), programmed PA continues to show substantial reductions in hypoglycemia with minimal impact on other metrics, whereas nonprogrammed PA exhibits smaller but directionally consistent improvements. Severe hyperglycemia remains rare, and total daily insulin delivery is comparable across targets.

Figs. 1 and 2 (bottom) illustrate stable cohort-level trajectories despite circadian IS variability, with the varying target maintaining clear anticipatory protection and tighter glucose envelopes around PA events.

## VI. CONCLUSION

In this work, we introduce an exercise-aware control strategy for the AP system based on a pulsatile zone MPC framework, designed to mitigate the risk of hypoglycemia associated with PA in individuals with Type 1 diabetes. Our approach elevates the glucose target zone dynamically (i.e., before, during, and after the announced PA event) by using a simple, deterministic mapping derived from the scheduled exercise. This not only implements clinically recommended practice directly into the controller architecture but does so in a way that makes the intervention transparent and interpretable for healthcare professionals.

The *in silico* results indicate that the proposed framework enhances glycemic safety across realistic and challenging scenarios. When compared to a standard fixed-target controller, the dynamic target elevation reduces both the incidence and duration of hypoglycemic episodes, while maintaining overall glycemic control. Notably, when the time-varying target zone modulation is combined with a model that explicitly accounts for PA effects, the overall control achieves substantial improvements in safety outcomes. In programmed PA scenarios, the framework obtains near-total elimination of severe hypoglycemia, significantly reduces the percentage of time spent below 70 and 54 mg/dL, while incurring only a modest increase in mean glucose and time above range. For nonprogrammed PA events, the improvements are more modest yet still clinically meaningful, further confirming the safety margins provided by the adaptive target strategy. This dual benefit highlights the synergistic effect of combining predictive target adjustments with PA-informed metabolic modeling.

It is worth noting, however, that although results do not consistently achieve optimal glycemic metrics under all conditions (i.e., total removal of PA-induced hypoglycemic events), the application of this exercise-aware target elevation stands out as a robust safety feature for preventing exercise-induced hypoglycemia. The controller's structure is capable of being used not only around PA windows but, with further development, throughout the day in synergy with additional behavioral/external signals, such as IOB profiles or glucose rate of change. In this way, it offers an alternative to methods that dynamically tune controller weights online [39];

unlike those approaches, which may compromise the problem's cost function continuity, our method maintains both continuity and convexity, resulting in stable, reliable performance. Finally, it is worth noting that the LTI model used is a simplification that does not fully capture the complex glucose–insulin dynamics. As a result, model–plant mismatch is inevitable in practice, arising from partially or absent announcements of meals and PA, as well as from unmodeled factors such as CGM sensor noise and delays, stress, hormonal variations, and intra- and intersubject physiological differences. Alternative approaches can address this issue explicitly through robust control formulations that account for bounded uncertainty, such as tube-based MPC strategies [40]. In this work, however, these discrepancies are mitigated through an offset-free state estimator that compensates for unmodeled dynamics and constant disturbances [9]. In addition, the use of soft constraints with slack variables, described in Section IV-A, avoids infeasibility during sudden metabolic transients. Together with patient-specific personalization of the model parameters, these features help maintain stable and safe glycemic regulation despite the model simplifications.

Nevertheless, several limitations and opportunities for further improvement should be highlighted. First, this study was conducted on a limited cohort of ten virtual adults, constrained by the commercial version of the UVA/Padua simulator [30]. Future investigations would benefit from evaluation on larger and more diverse populations. Furthermore, the adolescent and pediatric age groups were not included in this analysis, as the simulator was validated exclusively on the adult population. Given that meal habits, IS patterns, and metabolic responses differ considerably between age groups, a single controller approach may prove suboptimal across the entire T1D population, warranting age-specific adaptations in future work. While the simulations incorporated various uncertainties in activity and meal announcements as well as circadian sensitivity variations, the IS profiles used were limited to those described in [37]. Additional sensitivity patterns, such as those proposed by Visentin et al. [41], should be explored to assess controller robustness under a broader range of metabolic conditions. Moreover, further refinement could be achieved by integrating adaptive, time-varying model sensitivities based on individual patient data or by incorporating model structure adaptations as demonstrated in recent works (e.g., the time-varying models [42] or nonlinear models [43]). Beyond IS, other sources of physiological variability should be considered in future studies, including the dawn phenomenon, inter- and inpatient variability in insulin pharmacokinetics parameters, and variability in meal absorption dynamics, among others. Finally, while this study demonstrates strong *in silico* performance, real-world applications would demand robust adaptation to sensor noise, patient-specific behavioral changes, and unforeseen or incorrectly announced PA patterns. Addressing these challenges will be critical to ensure the clinical viability and safety of the proposed framework. Overall, the proposed exercise-aware pZMPC framework provides a promising, interpretable, and effective solution for the safe management of exercise-related glycemic disturbances in AP systems. By automating clinically inspired target adaptation

TABLE VII  
MODEL PARAMETERS DESCRIPTION

Parameter	Description
$\theta_0$ [mg/(dL·min)]	Endogenous glucose production (EGP)
$\theta_1$ [1/min]	Glucose effectiveness
$\theta_2$ [mg/(dL·U)]	Insulin sensitivity
$\theta_3$ [mg/(dL·g)]	Carbohydrate factor
$\theta_4$ [min]	Insulin absorption time constant
$\theta_5$ [min]	Meals absorption time constant
$\theta_6$ [mg/dL]	Rate of BG utilization due to PA level
$\theta_7$ [min]	Time-to-maximum PA effect

directly within a predictive control structure, the approach maintains and reconciles safety-oriented clinical heuristics with the predictive strength of MPC; this integration of physiological insight and control theory represents a promising step toward safer, more reliable, and patient-tailored AP systems capable of handling the challenges posed by PA.

#### APPENDIX

The glucose–insulin system adopted in this work is based on the Ruan physiological long-term model [27]; in this proposal, we also adopt its extension presented in [10] to account for the insulin-independent effect of PA. Its dynamics are expressed in state-space form as

$$\begin{aligned} \dot{x}(t) &= Ax(t) + B_u u(t) + B_z z(t) + E \\ y(t) &= Cx(t) \end{aligned} \quad (16)$$

where  $x(t) \in \mathbb{R}^{n_x}$  collects the system states,  $u(t)$  is the insulin infusion [U/min] (the controlled input), and  $z(t)$  represents exogenous inputs (meals and PA). The output  $y(t) = x_1(t)$  corresponds to BG concentration [mg/dL]. The parameters describing both models' dynamics are detailed in Table VII.

##### A. Five-State Model

In Abuin et al. [9], the model does not account for the PA effect; hence, the only exogenous input is the meal signal, that is,  $z(t) = r(t)$ , represented as the rate of the carbohydrate (CHO) intake [g/min]. The state vector is  $x(t) = [x_1(t), x_2(t), x_3(t), x_4(t), x_5(t)]'$ , with  $x_1(t)$  being the BG concentration [mg/dL],  $x_2(t)$  being the insulin delivery rate in plasma [U/min],  $x_3(t)$  being the insulin delivery rate in the subcutaneous compartment [U/min],  $x_4(t)$  being the rate of carbohydrate absorption from the gut [g/min], and  $x_5(t)$  being the glucose delivery rate from the stomach [g/min].

The model matrices are given by

$$\begin{aligned} A &= \begin{bmatrix} -\theta_1 & -\theta_2 & 0 & \theta_3 & 0 \\ 0 & -\theta_4^{-1} & \theta_4^{-1} & 0 & 0 \\ 0 & 0 & -\theta_4^{-1} & 0 & 0 \\ 0 & 0 & 0 & -\theta_5^{-1} & \theta_5^{-1} \\ 0 & 0 & 0 & 0 & -\theta_5^{-1} \end{bmatrix} \\ B_u &= \begin{bmatrix} 0 \\ 0 \\ \theta_4^{-1} \\ 0 \\ 0 \end{bmatrix}, \quad B_z = \begin{bmatrix} 0 \\ 0 \\ 0 \\ \theta_5^{-1} \\ 0 \end{bmatrix}, \quad E = \begin{bmatrix} \theta_0 \\ 0 \\ 0 \\ 0 \\ 0 \end{bmatrix}, \quad C = \begin{bmatrix} 1 \\ 0 \\ 0 \\ 0 \\ 0 \end{bmatrix}^\top \end{aligned}$$

where  $\theta_1$  is the glucose effectiveness [ $\text{min}^{-1}$ ],  $\theta_2$  is the IS [mg/(dL · U)],  $\theta_3$  is the carbohydrate raising factor

[mg/(dL · g)], and  $\theta_0$  is the endogenous glucose production (EGP) [mg/(dL · min)] at basal levels  $EGP_b$ , with  $\theta_0 = \theta_1 G_b + \theta_2 U_b$  at basal glucose  $G_b$  and insulin rate  $U_b$ . The absorption kinetics are governed by  $\theta_4$  and  $\theta_5$  [min] corresponding, respectively, to the time-to-maximum effective insulin concentration, and time-of-maximum appearance rate of glucose in the gut.

##### B. Seven-State Model

In Licini et al. [10], the previous five-state model has been extended with two additional states describing the insulin-independent PA effect [44]. The exogenous inputs are now meals and PA, that is,  $z(t) = [r(t) \ p(t)]^\top$ . The PA subsystem is

$$\begin{aligned} \dot{x}_6(t) &= -\frac{1}{\theta_7} x_6(t) + \frac{1}{\theta_7} x_7(t) \\ \dot{x}_7(t) &= -\frac{1}{\theta_7} x_7(t) + \frac{1}{\theta_7} p(t). \end{aligned} \quad (17)$$

The effect enters in glycemia dynamics through  $\dot{x}_1(t) = \theta_0 - \theta_1 x_1(t) - \theta_2 x_2(t) + \theta_3 x_3(t) - \theta_6 x_6(t)$ , capturing the balance between increased muscular glucose utilization and reduced hepatic glucose production during PA, independently of insulin action. The full model matrices are

$$\begin{aligned} A &= \begin{bmatrix} -\theta_1 & -\theta_2 & 0 & \theta_3 & 0 & -\theta_6 & 0 \\ 0 & -\theta_4^{-1} & \theta_4^{-1} & 0 & 0 & 0 & 0 \\ 0 & 0 & -\theta_4^{-1} & 0 & 0 & 0 & 0 \\ 0 & 0 & 0 & -\theta_5^{-1} & \theta_5^{-1} & 0 & 0 \\ 0 & 0 & 0 & 0 & -\theta_5^{-1} & 0 & 0 \\ 0 & 0 & 0 & 0 & 0 & -\theta_7^{-1} & \theta_7^{-1} \\ 0 & 0 & 0 & 0 & 0 & 0 & -\theta_7^{-1} \end{bmatrix} \\ B_u &= \begin{bmatrix} 0 \\ 0 \\ \theta_4^{-1} \\ 0 \\ 0 \\ 0 \\ 0 \end{bmatrix}, \quad B_z = \begin{bmatrix} 0 & 0 \\ 0 & 0 \\ 0 & 0 \\ 0 & 0 \\ \theta_5^{-1} & 0 \\ 0 & 0 \\ 0 & \theta_7^{-1} \end{bmatrix}, \quad E = \begin{bmatrix} \theta_0 \\ 0 \\ 0 \\ 0 \\ 0 \\ 0 \\ 0 \end{bmatrix}, \quad C = \begin{bmatrix} 1 \\ 0 \\ 0 \\ 0 \\ 0 \\ 0 \\ 0 \end{bmatrix}^\top. \end{aligned}$$

*Remark 3:* The following remarks clarify personalization, discretization, and observability aspects of the model:

- (i) Personalization of the model (16) is performed via a regularized least-squares (RLS) parameter estimation routine, as in [9] for the five-state model and [10] for the seven-state one. Patient-specific values can be found therein.
- (ii) The model is discretized with sampling time  $T_s$  for predictive control. Since insulin pumps typically deliver microboluses of duration  $\Delta T$ , the pulsatile input scheme of [9] and [10] is adopted.
- (iii) Both models are fully observable, even though only BGL ( $x_1$ ) is directly measured. In practice, the state estimate  $\hat{x}(k)$  is obtained through an output disturbance observer (ODO), providing offset-free estimation under impulse, step, or ramp mismatches (details can be found in [9]).

## REFERENCES

- [1] A. Katsarou et al., "Type 1 diabetes mellitus," *Nature Rev. Disease Primers*, vol. 3, no. 1, p. 17016, Mar. 2017.
- [2] M. Messori, G. Paolo Incremona, C. Cobelli, and L. Magni, "Individualized model predictive control for the artificial pancreas: In silico evaluation of closed-loop glucose control," *IEEE Control Syst. Mag.*, vol. 38, no. 1, pp. 86–104, Feb. 2018.
- [3] G. L. Dohm, "Invited review: Regulation of skeletal muscle GLUT-4 expression by exercise," *J. Appl. Physiol.*, vol. 93, no. 2, pp. 782–787, Aug. 2002.
- [4] J. O. Holloszy, "Exercise-induced increase in muscle insulin sensitivity," *J. Appl. Physiol.*, vol. 99, no. 1, pp. 338–343, Jul. 2005.
- [5] J. R. Zierath, A. Krook, and H. Wallberg-Henriksson, "Insulin action and insulin resistance in human skeletal muscle," *Diabetologia*, vol. 43, no. 7, pp. 821–835, Jul. 2000.
- [6] M. C. Riddell et al., "Exercise management in type 1 diabetes: A consensus statement," *Lancet Diabetes & Endocrinol.*, vol. 5, no. 5, pp. 377–390, May 2017.
- [7] P. Abuin, A. Ferramosca, C. Toffanin, L. Magni, and A. H. González, "Pulsatile zone MPC with asymmetric stationary cost for artificial pancreas based on a non-standard IOB constraint," *J. Process Control*, vol. 136, Apr. 2024, Art. no. 103191.
- [8] C. D. Man, F. Micheletto, D. Lv, M. Breton, B. Kovatchev, and C. Cobelli, "The UVA/PADOVA type 1 diabetes simulator: New features," *J. Diabetes Sci. Technol.*, vol. 8, no. 1, pp. 26–34, Jan. 2014.
- [9] P. Abuin, P. S. Rivadeneira, A. Ferramosca, and A. H. González, "Artificial pancreas under stable pulsatile MPC: Improving the closed-loop performance," *J. Process Control*, vol. 92, pp. 246–260, Aug. 2020.
- [10] N. Licini, B. Sonzogni, P. Abuin, F. Previdi, A. H. Gonzalez, and A. Ferramosca, "Artificial pancreas under stable pulsatile model predictive control: Including the physical activity effect," in *Proc. IEEE 63rd Conf. Decis. Control (CDC)*, Dec. 2024, pp. 4028–4033.
- [11] R. C. Camacho, P. Galassetti, S. N. Davis, and D. H. Wasserman, "Glucoregulation during and after exercise in health and insulin-dependent diabetes," *Exercise Sport Sci. Rev.*, vol. 33, no. 1, pp. 17–23, 2005.
- [12] R. B. Batacan, M. J. Duncan, V. J. Dalbo, P. S. Tucker, and A. S. Fenning, "Effects of high-intensity interval training on cardiometabolic health: A systematic review and meta-analysis of intervention studies," *Brit. J. Sports Med.*, vol. 51, no. 6, pp. 494–503, Mar. 2017.
- [13] L. Bally, M. Laimer, and C. Stettler, "Exercise-associated glucose metabolism in individuals with type 1 diabetes mellitus," *Current Opinion Clin. Nutrition Metabolic Care*, vol. 18, no. 4, pp. 428–433, Jul. 2015.
- [14] American Diabetes Association, "Physical activity/exercise and diabetes mellitus," *Diabetes Care*, vol. 26, no. 1, pp. s73–s77, Jan. 2003.
- [15] S. Franc et al., "Insulin-based strategies to prevent hypoglycaemia during and after exercise in adult patients with type 1 diabetes on pump therapy: The diabraport randomized study," *Diabetes, Obesity Metabolism*, vol. 17, no. 12, pp. 1150–1157, 2015.
- [16] A. Jeukendrup, "A step towards personalized sports nutrition: Carbohydrate intake during exercise," *Sports Med.*, vol. 44, no. S1, pp. 25–33, May 2014.
- [17] T. Danne et al., "The PILGRIM study: In silico modeling of a predictive low glucose management system and feasibility in youth with type 1 diabetes during exercise," *Diabetes Technol. Therapeutics*, vol. 16, no. 6, pp. 338–347, Jun. 2014.
- [18] J. Pavan, G. Noaro, A. Facchinetti, D. Salvagnin, G. Sparacino, and S. Del Favero, "A strategy based on integer programming for optimal dosing and timing of preventive hypoglycemic treatments in type 1 diabetes management," *Comput. Methods Programs Biomed.*, vol. 250, Jun. 2024, Art. no. 108179.
- [19] N. Licini, B. Sonzogni, P. Abuin, F. Previdi, A. H. González, and A. Ferramosca, "Optimized carbohydrate suggestions and insulin dosing in artificial pancreas: Dual-action pulsatile zone MPC with non-standard IOB constraints for physical activity management," in *Proc. Eur. Control Conf. (ECC)*, Jun. 2025, pp. 564–569.
- [20] M. C. Riddell, D. P. Zaharieva, L. Yavelberg, A. Cinar, and V. K. Jamnik, "Exercise and the development of the artificial pancreas: One of the more difficult series of hurdles," *J. Diabetes Sci. Technol.*, vol. 9, no. 6, pp. 1217–1226, Nov. 2015.
- [21] M. Breton et al., "Fully integrated artificial pancreas in type 1 diabetes," *Diabetes*, vol. 61, no. 9, pp. 2230–2237, Sep. 2012.
- [22] A. Haidar, M. R. Smaoui, L. Legault, and R. Rabasa-Lhoret, "The role of glucagon in the artificial pancreas," *Lancet Diabetes Endocrinol.*, vol. 4, no. 6, pp. 476–479, Jun. 2016.
- [23] A. Weisman, J.-W. Bai, M. Cardinez, C. K. Kramer, and B. A. Perkins, "Effect of artificial pancreas systems on glycaemic control in patients with type 1 diabetes: A systematic review and meta-analysis of outpatient randomised controlled trials," *Lancet Diabetes Endocrinol.*, vol. 5, no. 7, pp. 501–512, Jul. 2017.
- [24] A. C. van Bon et al., "Bihormonal fully closed-loop system for the treatment of type 1 diabetes: A real-world multicentre, prospective, single-arm trial in The Netherlands," *Lancet Digit. Health*, vol. 6, no. 4, pp. e272–e280, Apr. 2024.
- [25] P. I. Beato-Víborá and F. J. Arroyo-Díez, "New uses and formulations of glucagon for hypoglycaemia," *Drugs Context*, vol. 8, pp. 1–10, Jul. 2019.
- [26] C. Furió-Novejarque et al., "Modeling the effect of glucagon on endogenous glucose production in type 1 diabetes: On the role of glucagon receptor dynamics," *Comput. Biol. Med.*, vol. 154, Mar. 2023, Art. no. 106605.
- [27] Y. Ruan, M. E. Wilinska, H. Thabit, and R. Hovorka, "Modeling day-to-day variability of glucose–insulin regulation over 12-week home use of closed-loop insulin delivery," *IEEE Trans. Biomed. Eng.*, vol. 64, no. 6, pp. 1412–1419, Jun. 2017.
- [28] P. Krupa et al., "Model predictive control for tracking using artificial references: Fundamentals, recent results and practical implementation," in *Proc. IEEE 63rd Conf. Decis. Control (CDC)*, Dec. 2024, pp. 2977–2991.
- [29] M. N. Zeilinger, M. Morari, and C. N. Jones, "Soft constrained model predictive control with robust stability guarantees," *IEEE Trans. Autom. Control*, vol. 59, no. 5, pp. 1190–1202, May 2014.
- [30] *DMMS.R*, T. E. Group, Schaffhausen, Switzerland, 2016.
- [31] M. Schiavon, C. D. Man, Y. C. Kudva, A. Basu, and C. Cobelli, "In silico optimization of basal insulin infusion rate during exercise: Implication for artificial pancreas," *J. Diabetes Sci. Technol.*, vol. 7, no. 6, pp. 1461–1469, Nov. 2013.
- [32] J. Lofberg, "YALMIP: A toolbox for modeling and optimization in MATLAB," in *Proc. IEEE Int. Conf. Robot. Autom.*, Sep. 2004, pp. 284–289.
- [33] S. R. Colberg et al., "Physical activity/exercise and diabetes: A position statement of the American Diabetes Association," *Diabetes Care*, vol. 39, no. 11, pp. 2065–2079, Nov. 2016.
- [34] M. Vettoretti, A. Facchinetti, G. Sparacino, and C. Cobelli, "Type-1 diabetes patient decision simulator for in silico testing safety and effectiveness of insulin treatments," *IEEE Trans. Biomed. Eng.*, vol. 65, no. 6, pp. 1281–1290, Jun. 2018.
- [35] M. MiniMed, "MiniMed 640G system user guide," *Medtronic*, p. 315, 2015.
- [36] American Diabetes Association, "6. Glycemic targets: Standards of medical care in diabetes—2019," *Diabetes Care*, vol. 42, no. 1, pp. S61–S70, Dec. 2018.
- [37] C. Toffanin, H. Zisser, F. J. Doyle, and E. Dassau, "Dynamic insulin on board: Incorporation of circadian insulin sensitivity variation," *J. Diabetes Sci. Technol.*, vol. 7, no. 4, pp. 928–940, Jul. 2013.
- [38] T. Danne et al., "International consensus on use of continuous glucose monitoring," *Diabetes Care*, vol. 40, no. 12, pp. 1631–1640, Dec. 2017.
- [39] M. Moscoso-Vásquez, J. Garcia-Tirado, P. Colmegna, and M. Breton, "Reshaping model predictive control penalties for an automated insulin delivery system in type 1 diabetes," *IFAC-PapersOnLine*, vol. 56, no. 2, pp. 9660–9665, 2023.
- [40] N. Licini, M. A. Santos, F. Previdi, and A. Ferramosca, "A robust tube-based MPC approach for safer insulin dosing," *IFAC J. Syst. Control*, vol. 35, Mar. 2026, Art. no. 100393.
- [41] R. Visentin, C. D. Man, Y. C. Kudva, A. Basu, and C. Cobelli, "Circadian variability of insulin sensitivity: Physiological input for in silico artificial pancreas," *Diabetes Technol. Therapeutics*, vol. 17, no. 1, pp. 1–7, Jan. 2015.
- [42] P. Abuin, A. Ferramosca, C. Toffanin, L. Magni, and A. H. Gonzalez, "Artificial pancreas under periodic MPC for trajectory tracking: Handling circadian variability of insulin sensitivity," *IFAC-PapersOnLine*, vol. 55, no. 16, pp. 196–201, 2022.
- [43] N. Licini, B. Sonzogni, P. Abuin, F. Previdi, A. H. González, and A. Ferramosca, "A novel dynamic modeling of insulin sensitivity in the blood glucose minimal model," in *Proc. Amer. Control Conf. (ACC)*, Jul. 2025, pp. 2029–2034.
- [44] D. Romeres, M. Schiavon, A. Basu, C. Cobelli, R. Basu, and C. Dalla Man, "Exercise effect on insulin-dependent and insulin-independent glucose utilization in healthy individuals and individuals with type 1 diabetes: A modeling study," *Amer. J. Physiol.-Endocrinol. Metabolism*, vol. 321, no. 1, pp. E122–E129, Jul. 2021.